Trends in Chemistry

CellPress OPEN ACCESS

Review

The chemistry of chemically fueled droplets

Carsten Donau[1] and Job Boekhoven [1,*]

Liquid compartments without a surrounding membrane control vital functions and chemistries in living cells. One subset of droplets regulated by chemical reactions is chemically fueled droplets. The phase-separating molecules that form these droplets are activated and deactivated by a reaction cycle that consumes a high-energy molecule (i.e., a chemical fuel). That means that the droplet exists out of equilibrium at the expense of chemical energy. This review aims to demonstrate how to design chemically fueled droplets and which types of unique behaviors can be expected. We highlight experimental advances that are corroborated by theory. We close the review with an outlook and aim to bridge the gap between theoreticians and experimentalists to build better liquid droplet models.

Highlights

Liquid droplets regulated by chemical reactions are critical in organizing cellular processes. They could have been critical compartments at the origin of life, too.

Chemically fueled droplets are an excellent model to study droplets inside cells.

Experimental and theory-based studies on chemically fueled droplets show exciting behaviors vastly different than close-to-equilibrium droplets.

Chemically fueled droplets are powerful for understanding better how biology uses and regulates liquid droplets.

Chemically fueled droplets

Phase separation of two immiscible liquids is common in our daily lives. A typical example is the oil droplets that separate from vinegar in an emulsion, a vinaigrette. The thermodynamics of these processes is well understood [1–3]. Recently, it was discovered that phase separation is also ubiquitous in biology. These droplets in the cell (i.e., lipid organelles [4] and biomolecular condensates [5]) are frequently actively maintained away from equilibrium by chemical reactions [6–14] and malfunction in their properties, such as liquidity or size, is correlated to disease [15–21]. Coupling phase separation to chemical reactions endows droplets with properties that differ from the well-understood behavior in equilibrium. For example, a gradient of proteins can control where phase separation occurs, leading to a controlled distribution of organelles along the cell [22,23]. However, the exact details of the governing mechanism of phase separation inside cells controlled by chemical reactions remain elusive [24–26].

A class of such actively maintained droplets is **chemically fueled droplets** (see Glossary). Theoretical and experimentalists' work is shedding light on the fundamentals of these chemically fueled droplets, allowing us to generalize some of their behaviors. We define 'chemically fueled droplets' as droplets in which the phase separating molecules are regulated by a chemically fueled reaction cycle (Figure 1). This cycle comprises a minimum of two reactions: (i) an **activation** reaction that activates a building block for phase separation at the expense of chemical fuel, and (ii) a **deactivation** reaction that reacts the activated building block back to the building block (Figure 1A). Thus, building blocks are temporarily activated for phase separation at the expense of the chemical fuel [27]. In the finite time the building blocks are active they diffuse into a droplet. The building block leaves the droplet when deactivated (Figure 1B). Consequently, chemically fueled droplets in a steady state look like passive droplets close to equilibrium, in that the concentrations of the activated building blocks are constant. However, the continuous activation and deactivation lead to atypical fluxes over the droplet interface, which gives rise to exciting, non-equilibrium behavior vastly different from their passive analogs. For example, it has been predicted that chemically fueled droplets can resist **Ostwald ripening** and evolve to a stable droplet size [28–30]. Under other conditions, these droplets can even self-divide [31,32]. Furthermore, another design shows that the ripening of these droplets can be accelerated by tuning the reaction rates

[1]Department of Chemistry, Technical University of Munich, Lichtenbergstrasse 4, 85748 Garching, Germany

*Correspondence: job.boekhoven@tum.de (J. Boekhoven).

© 2022 The Author(s). Published by Elsevier Inc. This is an open access article under the CC BY-NC-ND license (http://creativecommons.org/licenses/by-nc-nd/4.0/).

[33]. Because rates of reactions and diffusion constants regulate these unique properties, they are not limited to one droplet type. Indeed, the building blocks for chemically fueled droplets can be small molecules, peptides, or proteins. Chemically fueled droplets are non-equilibrium droplets and have also been referred to by others as 'active droplets'. We prefer to reserve the term chemically fueled droplets as it sets them apart from other types of active matter (e.g., self-propelled active droplets) [34,35].

Synthetic strategies towards chemically fueled droplets are reported based on oil- and coacervate-based droplets. Coacervate droplets are considered a relevant protocell model at the origin of life because their aqueous interior allows compartmentalizing prebiotic metabolic pathways [36,37]. More detailed studies of chemically fueled droplets thus offer insight into the fundamental behavior of the cell's phase-separated organelles and prebiotic compartments.

We have established four possible designs of chemically fueled droplets depending on where activation and deactivation predominantly occur concerning the droplet (Figure 1B). While molecules will usually be present in both phases during experiments, partitioning a molecule between the phases will determine whether a reaction is occurring predominantly inside or outside the droplets. Either the reactions are separated by the droplet boundary, that is, the activation occurs outside whereas deactivation occurs in the droplet (Figure 1, design 1), or activation occurs in the droplet and deactivation outside (Figure 1, design 2). Alternatively, both reactions are localized outside the droplet (Figure 1, design 3), or both occur within the droplet (Figure 1, design 4). We have established here that each of these designs comes with unique properties. We will review these cases and illustrate what experimental and theoretical efforts have been made to understand such chemically fueled droplets.

To limit the scope of this review, we will describe exclusively chemically fueled droplets following strictly the aforementioned definition (activation and deactivation of building blocks at the expense of fuel take place simultaneously). Other droplet systems regulated by chemical reactions exist and exhibit exciting behavior too. These include reactions that activate or deactivate building blocks by light-driven reactions [38–41], redox chemistry [42–44], changes in pH [45–55], enzymes [56–65], and others [66–72]. Because in these studies, activation and deactivation do not take place simultaneously, a steady state cannot be reached and these droplets are thus endowed with very different rules compared to chemically fueled droplets. The reader is referred to excellent reviews on such systems [73–76].

Glossary

Activation: building block precursors are activated for phase separation by a fuel-driven chemical reaction.
Autocatalytic droplet: a droplet accelerates the activation reaction (i.e., the formation of new activated building blocks). In other words, the larger a droplet, the more it helps to synthesize its building blocks.
Chemically fueled droplets: droplets whose building blocks are regulated by a fuel-driven chemical reaction cycle (i.e., a fuel-driven activation and spontaneous deactivation reaction).
Deactivation: activated droplet building blocks are deactivated for phase separation through a spontaneous chemical reaction.
Laplace pressure: pressure between the inside and outside of the droplet interface that is caused by surface tension.
Ostwald ripening: thermodynamic process that reduces the total droplet surface area. Specifically, large droplets grow at the expense of smaller ones driven by Laplace pressure differences between the droplets.
Stationary size: the optimal droplet size in a system where droplet building blocks are regulated by chemical reactions. At this size, influx and efflux of building blocks are balanced.
Supersaturation: excess concentration of activated building blocks above the saturation level in the dilute phase.

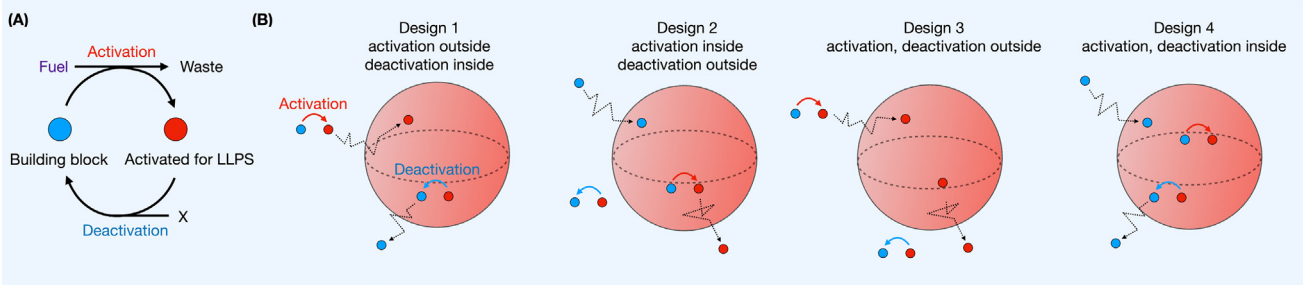

Figure 1. Design of chemically fueled droplets. (A) A chemical reaction cycle transiently activates a building block (blue disk) for liquid–liquid phase separation (LLPS) at the expense of chemical fuel. The activated building block (red disk) can phase-separate in its finite lifetime, resulting in droplet formation until it is deactivated by a ubiquitous molecule X. (B) Four designs of chemically fueled droplets. Each droplet is regulated by chemically fueled activation and spontaneous deactivation simultaneously. The designs differ in where the reactions take place.

Design 1: activation outside and deactivation inside

We first discuss the design where droplet building blocks are activated outside the droplet and deactivated inside (Figure 2A). Such a design has the unique property that most of the activated building blocks need to diffuse into a droplet before they can be deactivated. Similarly, most of the deactivated building blocks leave the droplet before they are reactivated. Therefore, the droplet is endowed with influxes and effluxes that are regulated by the kinetics of the chemical reaction cycle. In such a design, one exciting property arises from the kinetics of the influx and efflux. That is, droplets all evolve to one preferred size that is dependent on the rate of deactivation. Simply put, the greater the droplet volume, the more activated building blocks it contains. Since the deactivation scales linearly with the number of activated building blocks, it will also scale linearly with the volume of the droplet. A molecule that is deactivated diffuses out of the droplet. As a result, the efflux of deactivated building blocks scales with the volume of the droplet. In contrast, the influx of activated droplet building blocks scales with its surface area. Simply put, a molecule is activated outside the dilute phase, after which it diffuses until it enters a droplet. The greater the droplet surface area, the more activated building blocks enter the droplet.

Because of the surface-area-dependent influx and volume-dependent efflux, all droplets evolve to one optimal size [28,30]. Droplets smaller than this optimal size will grow. In contrast, droplets larger than this size will shrink. Droplets in an emulsion close to equilibrium differ vastly from such chemically fueled droplets [30]. The undesirable interfacial energy between the droplets and their surrounding media means that an emulsion close to equilibrium aims to decrease its surface area, a process that is called coarsening. To coarsen, droplets can either fuse or undergo Ostwald ripening. Ostwald ripening is a process driven by **Laplace pressure** differences between droplets [30]. Specifically, the Laplace pressure of tiny droplets is higher compared with larger droplets. This pressure difference leads to a concentration gradient of droplet molecules from smaller to larger droplets, ultimately resulting in larger droplets growing at the expense of smaller ones. Therefore, coarsening results in a continuous increase in the droplet radius, which can be calculated as demonstrated in Figure 2B [30]. Here, the growth rate (i.e., the change in the droplet size over time) is dependent on the size of the droplet. In passive droplets close to equilibrium (Figure 2B, blue trace), tiny droplets above a nucleation threshold grow quickly, whereas droplets below this value are not stable and dissolve. Very big droplets grow continuously, dependent on the system size.

In contrast, droplets of design 1 (Figure 2B, orange trace) can suppress Ostwald ripening to favor many droplets around the critical volume [28]. Indeed, calculations show that droplets below the **stationary size** grow (Figure 2B), whereas droplets bigger than the stationary size have a negative growth rate and shrink (Figure 2B). This unique property was demonstrated in a simulation depicted in Figure 2C [77]. Close to equilibrium, passive droplets ripen into a few large droplets through Ostwald ripening. In contrast, multiple chemically fueled droplets of design 1 coexist and grow towards an optimal volume at a steady state.

While droplets that are not regulated by chemical reactions typically maintain a spherical shape due to surface tension effects, diffusive fluxes in a chemically fueled droplet with a very large stationary size can deform the droplet once a critical size is reached [78]. Since the influx of newly activated building blocks scales with the surface area and is more favorable at a high mean curvature, shape instabilities lead to the continuous elongation of a deformed droplet (Figure 2D) [30]. Conversely, the efflux of deactivated droplet building blocks outcompetes the influx in the middle part of the droplet due to a lower mean curvature. These imbalances in the diffusive fluxes result in separating the large, deformed droplet into two smaller droplets of spherical shape (Figure 2E) [31,32]. This self-division process can repeat itself via regrowth of the newly

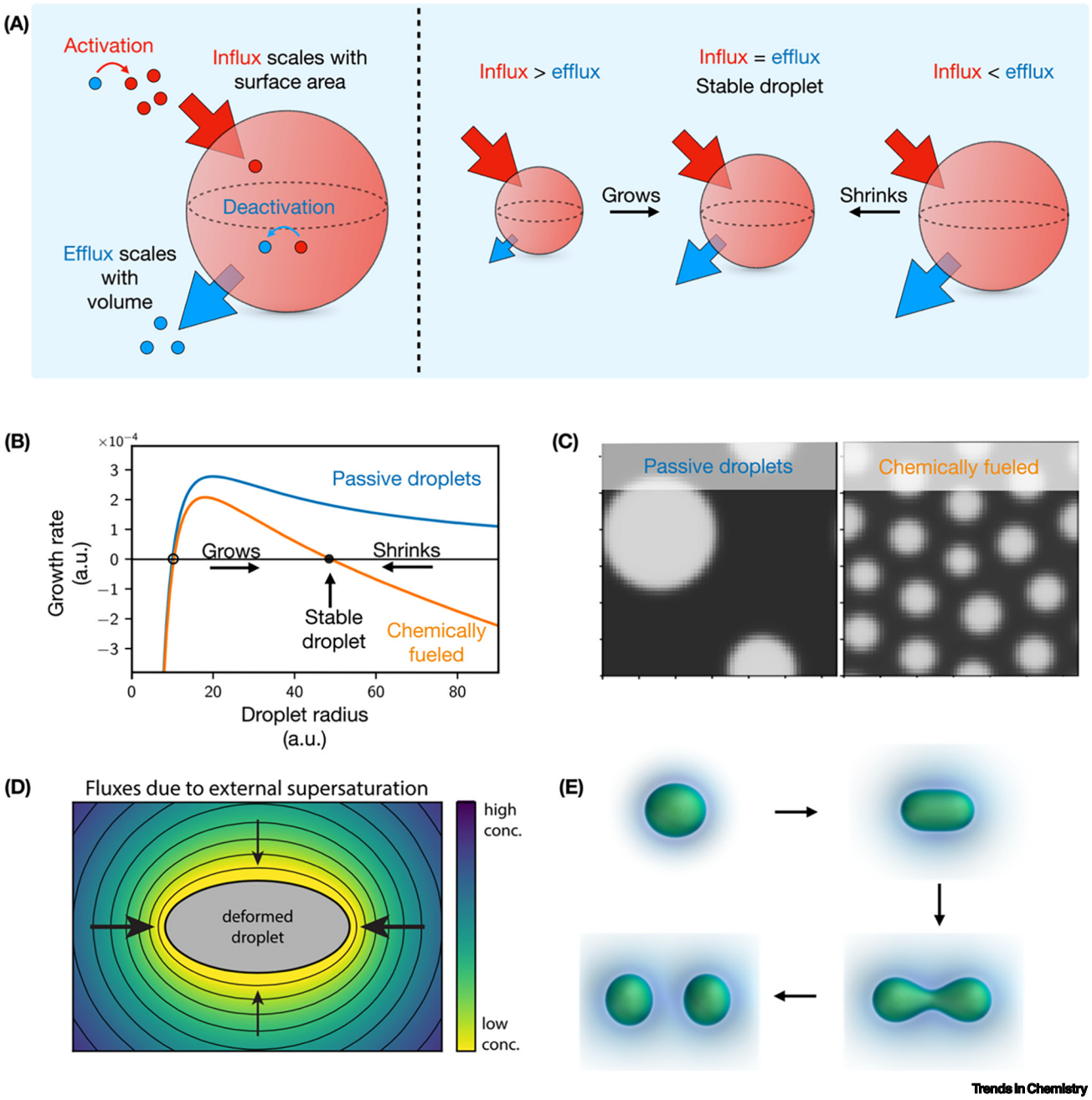

Figure 2. Theoretical simulations of droplets following design 1. (A) Schematic representation of a chemically fueled droplet where activated building block (red disk) is deactivated (blue disk) inside and reactivated outside the droplet. The balance between surface-dependent influx (red arrow) and volume-dependent efflux (blue arrow) regulates whether a droplet grows or shrinks. Small droplets have a high surface-to-volume ratio and thus grow. In contrast, large droplets have a low surface-to-volume ratio and shrink. At a specific intermediate size, influx and efflux are balanced. As a result, this droplet size is stable and all droplets converge to this size eventually. (B) The growth rate of passive (blue) and chemically fueled droplets (orange) as a function of the droplet size. Stationary states are shown for stable (filled circle) and unstable (empty) states. Passive droplets grow infinitely until the system size is reached, whereas chemically fueled droplets stabilize around a stationary size. Adapted, with permission, from [30]. (C) Numerical simulations of passive (left) and chemically fueled droplets (right) by design 1. Adapted, with permission, from the author [77]. (D) Chemical fluxes in a deformed chemically fueled droplet. When the stationary size of chemically fueled droplets is large, shape deformations can occur. The influx of activated building blocks is then favored at the droplet surface with high mean curvature (left and right side of the deformed droplet), whereas efflux is favored at low mean curvature (top and bottom). As a result, the droplet elongates continuously. Adapted, with permission, from [30]. (E) Simulation of the self-division of a chemically fueled droplet. Adapted, with permission, from [31].

formed droplets until the **supersaturation** is sufficiently depleted [30]. This finding is remarkable, given the simplicity of the droplet system, and serves as an inspiring example of how chemical reactions can alter droplet behavior.

Two reported droplet systems are conceptually similar to design 1 (i.e., droplet building blocks are activated outside and deactivated within the droplet). Fanalista and colleagues designed complex coacervate droplets that form when guanosine triphosphate (GTP) and polylysine are mixed in a PDMS-based microchamber (Figure 3A) [79]. When the authors added FtsZ, a tubulin homolog in bacteria that uses GTP to assemble into filaments [80], it preferentially localized on the coacervates' surface. Since FtsZ catalyzes GTP hydrolysis to GDP, it catalyzes the deactivation. Indeed, the droplets were unstable in the presence of FtsZ and shrunk in tens of minutes (Figure 3B) [79]. The total consumption of GTP did not entirely dissolve the droplets but left behind aggregates hypothesized to comprise FtsZ, GDP, and polylysine. Next, the authors supplied GTP from the dilute phase by flushing fresh GTP through the microchamber. In other words, new droplet building blocks were supplied from the outside and deactivated inside the droplets. Indeed, droplets could be stabilized, resulting in stable droplet sizes for more than an hour (Figure 3C) [79]. Even though the droplets most probably remained polydisperse, this example shows that droplets regulated by spatial fluxes and chemical reactions can stabilize if the droplet boundary's chemical fluxes are balanced. Finally, the authors show that coupling the deactivation of building blocks to the formation of filaments on the droplets' surface may lead to morphological transitions (e.g., when the droplets are exposed to mechanical stress; Figure 3D) [79].

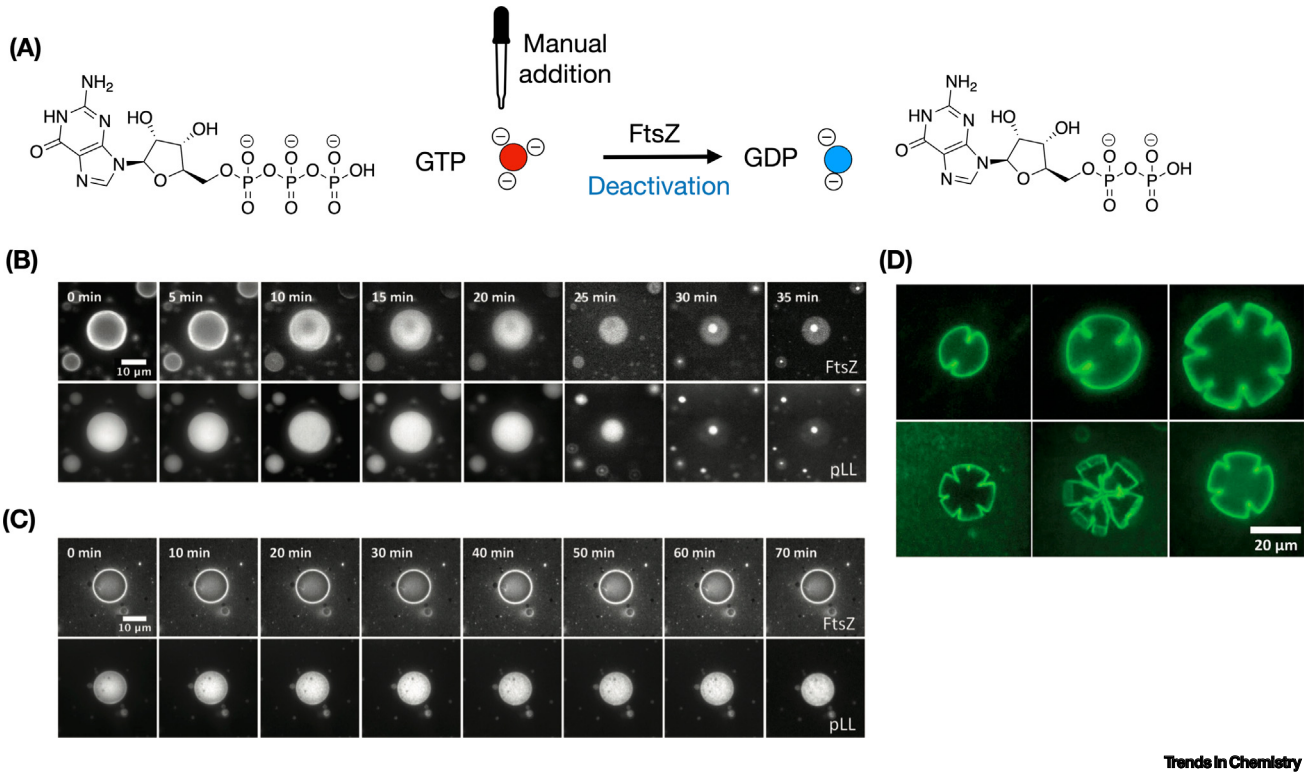

Figure 3. GTP-fueled droplets following design 1. (A) Deactivation of GTP to GDP by adding FtsZ results in the deactivation of coacervate building blocks [79]. (B,C) Microscopic images of the droplet evolution with no (B) or continuous (C) supply of GTP from the outside [79]. Due to the continuous deactivation of GTP to GDP, droplets shrink drastically (B). The droplets can be stabilized by the continuous supply of GTP (C). (D) Shape deformations of droplets from (A) under mechanical stress [79]. (B–D) Adapted, with permission, from [79].

Boekhoven and colleagues also introduced a droplet system following design 1 (Figure 4A) [81]. They used a chemical reaction cycle that converts a C-terminal aspartic acid into its anhydride state by consuming a carbodiimide-based fuel (fuel-driven activation). That anhydride hydrolyzes back to aspartic acid spontaneously (deactivation). When designed in an arginine-containing peptide, the building block has a low affinity for RNA. However, upon fuel-driven activation, the peptide loses its two negative charges, which increases its affinity for RNA (Figure 4A,B). Thus, the activated building block can bind RNA, which induces coacervate droplet formation. Because the deactivated building block has a poor affinity for RNA, it primarily resides outside the droplets. As a result, the activation occurs mostly outside. Because of the activated building block's high affinity for RNA, it primarily resides inside the droplets, and deactivation mainly occurs within

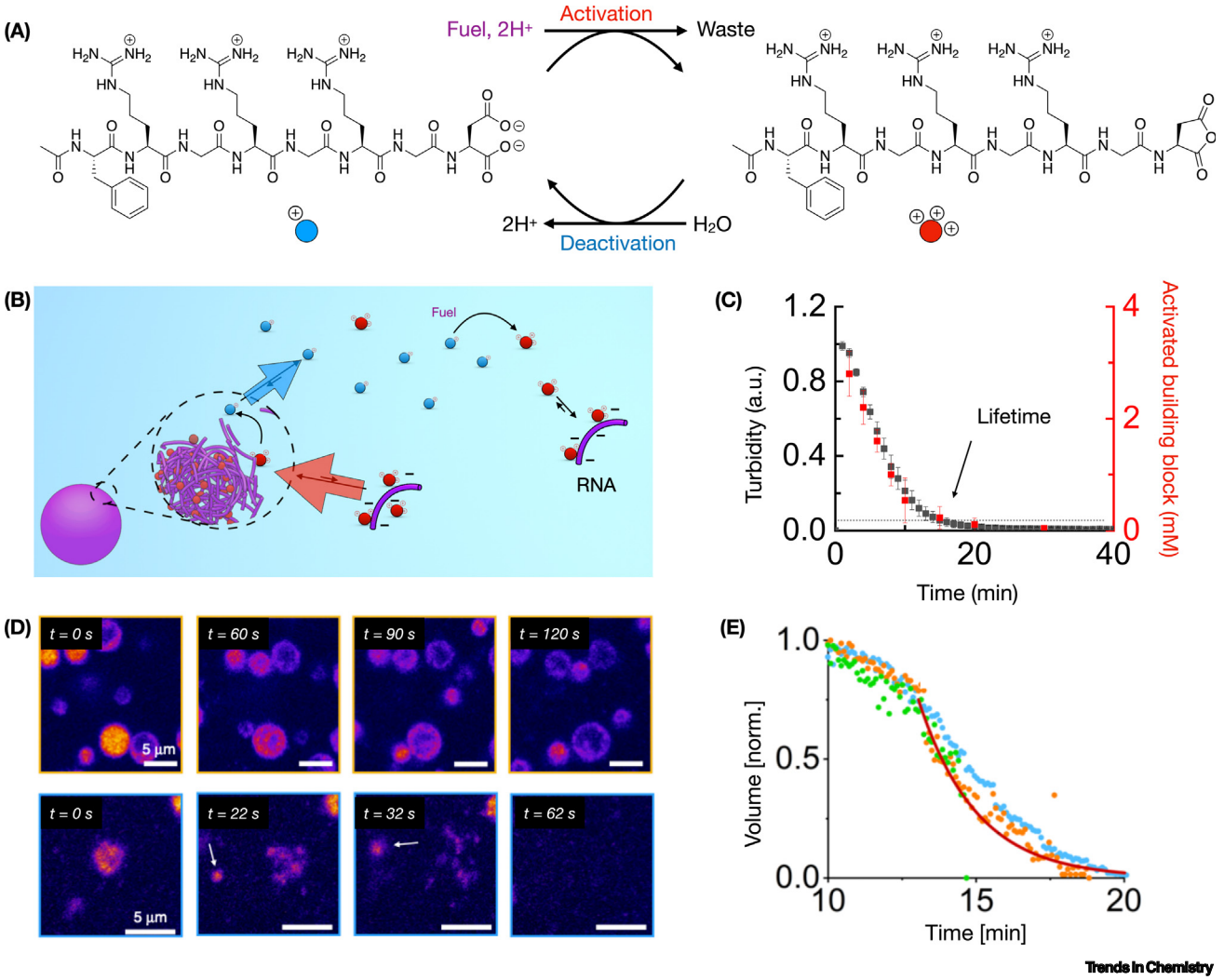

Figure 4. Carbodiimide-fueled droplets following design 1. (A) A chemical reaction cycle that converts a chemical fuel (EDC) into waste (EDU) while transiently removing two negative charges on a building block [81]. (B) Schematic representation of complex coacervate droplets from (A) composed of RNA and a chemically fueled peptide following design 1. The loss of two negative charges increases the peptide's positive net charge, leading to an increased affinity to complex RNA, resulting in droplets. The peptide loses its affinity for RNA upon deactivation inside the droplet, resulting in the efflux of molecules. (C) Turbidity (black) and concentration of activated building block (red) as a function of time when 25 mM fuel is added as a batch [81]. (D) Microscopic images of the fusion, vacuole formation, and fragmentation of droplets when fuel is scarce [81]. (C,D) Adapted, with permission, from [81]. (E) Normalized droplet volume of three droplets with different sizes as a function of time. The red line represents a fit using the deactivation rate constant of the activated building block. Adapted, with permission, from [83].

the droplets (Figure 4B). Consequently, the droplet is regulated by the kinetics of the reaction cycle and the amount of fuel added.

Indeed, in response to fuel, the evolution of the droplets was tightly regulated by the reaction cycle. The turbidity of the sample, which is a measure of the presence of droplets, evolved similarly to the concentration of the activated building block (Figure 4C) [81]. The chemically fueled droplets rapidly grew via fusion and decayed after 20 min because all fuel was consumed. During this decay process, these dynamic droplets showed unexpected behavior, including vacuolization and irregular droplet division into tiny droplet fragments (Figure 4D) [81]. The authors hypothesized that, as the deactivation was outcompeting the activation towards the end of the reaction cycle, the increase in unfavorable interactions inside the droplet would lead to the efflux of molecules and droplet disassembly. A follow-up study demonstrated that when polystyrene sulfonate was used as a polyanion instead of RNA, these droplets did not self-divide [82,83]. Instead, they tended to shrink as the system ran out of chemical fuel. Excitingly, the droplet's dissolution kinetics matched the deactivation kinetics accurately, further demonstrating that the droplet properties are regulated through the kinetics of the reaction cycle (Figure 4E) [83]. In all these experiments, the droplets are fueled with a batch of chemical fuel and never reach a steady state as in the theoretical simulations. Therefore, to find size-control behavior based on design 1, these droplets should be kept in a steady state.

Design 2: activation inside and deactivation outside

In design 2, the activation occurs within the droplet, whereas deactivation is predominantly outside (Figure 5A). A theory-based study on such a design describes an **autocatalytic droplet** catalyzing the activation of its building blocks [28,84]. The activation is, therefore, volume-dependent (i.e., a large droplet synthesizes more building blocks than a small one). The influx of building blocks is coupled to the activation reaction (i.e., when a building block is activated, the droplet can partition a new, not yet activated building block). As a result, the influx of building blocks into the droplet is also volume-dependent. In contrast, the efflux of activated building blocks into the dilute phase depends on the droplet's surface area. On the one hand, big droplets with a small surface area to volume ratio will grow faster than small ones. On the other hand, tiny droplets will shrink due to a high surface area-to-volume ratio. Thus, tiny droplets will dissolve and large droplets will grow. This behavior is reminiscent of Ostwald ripening but occurs faster than droplets close to equilibrium [28,84]. In other words, the fuel-driven chemical reaction cycle can accelerate droplet ripening.

While these autocatalytic droplets can grow exponentially once they cross a critical radius, their nucleation is inherently difficult, considering the activated building blocks are not produced without droplets [84]. A method to decrease this nucleation barrier is by incorporating an active core that catalyzes the activation (e.g., by the localization of an enzyme; Figure 5B). Here, the activation of building blocks via a catalytic activity Q is dependent on the core's relative volume and far less on the size of the droplet, in contrast to purely autocatalytic droplets. Therefore, the limiting factor for droplet growth is the influx of deactivated building blocks, which favors the growth of smaller droplets and shrinkage of larger ones. Like design 1, stable droplet size is obtained when influxes and effluxes are matched, leading to suppressed Ostwald ripening and multiple droplets coexisting at a stationary size [28,30,84]. Interestingly, droplets of unequal sizes can coexist if they possess disparate catalytic activities in the active core [28]. Furthermore, activation and deactivation in such autocatalytic droplets can regulate the positioning of particles within the droplet [85]. The growth rates of such autocatalytic droplets are depicted in Figure 5C [28]. An autocatalytic droplet will grow until the system size is reached (blue trace). In contrast, an autocatalytic

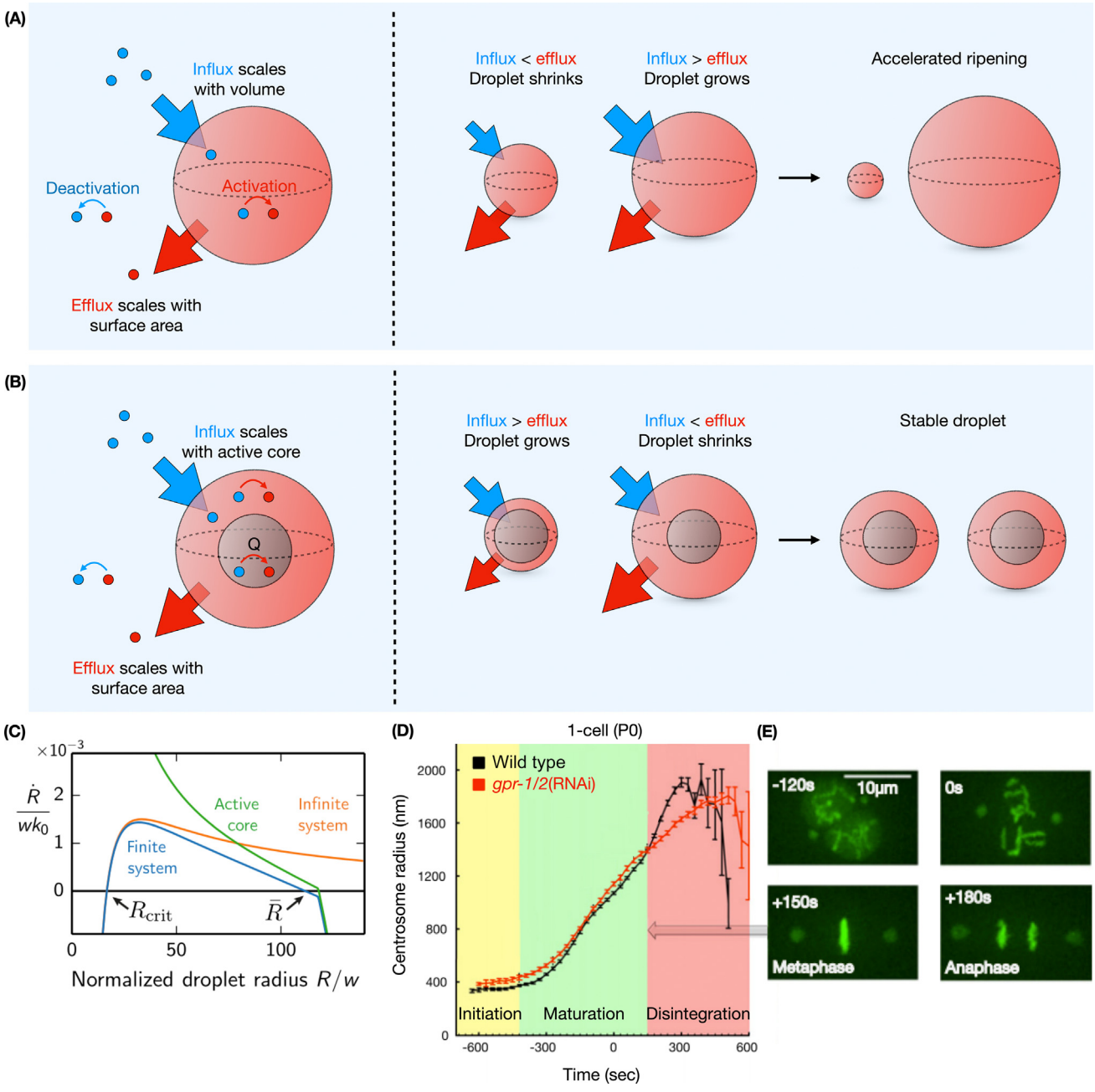

Figure 5. Chemically fueled droplets whose building blocks are being activated inside and deactivated outside following design 2. (A) Schematic representation of an autocatalytic droplet where an activated building block catalyzes its formation in the droplet, whereas deactivation occurs outside [28,84]. The balance between volume-dependent influx (blue arrow) and surface-dependent efflux (red arrow) regulates whether a droplet grows or shrinks. Small droplets have a high surface-to-volume ratio and thus shrink. In contrast, large droplets have a low surface-to-volume ratio and grow. As a result, larger droplets grow at the expense of smaller ones, similar to Ostwald ripening but accelerated. (B) The autocatalytic droplet from (A) contains an active core with a catalytic activity Q [28,84]. The core's relative size is decisive for droplet shrinkage and growth, resulting in droplets coexisting at a stable size. (C) The growth rate as a function of the droplet size [28]. Profiles of autocatalytic droplets in a finite (blue) and infinite (orange) system and autocatalytic droplets with an active core in a finite system (green) are shown. Autocatalytic droplets with an active core (green) nucleate easier than autocatalytic droplets without an active core (blue). Adapted, with permission, from [28]. (D) Centrosome radius over time of wild types and gpr-1/2(RNAi) embryos [86]. Error bars are the standard error of the mean. (E) The image sequence of embryos expressing both g-tubulin::GFP and histone::GFP illustrates the formation of the centrosomes and mitotic spindle. (D,E) Adapted, with permission, from [86].

droplet with an active core (green trace) has a shallow nucleation barrier and, thus, small droplets grow considerably faster than droplets without an active core. These droplets then grow until the system size is reached as well. In an infinite system (orange trace), autocatalytic droplets behave like passive droplets (Figure 2B).

An example of how active cores can regulate droplet growth comes from centrosomes [86], which are liquid-like droplets in the cell nucleus that are crucial for the positioning of the mitotic spindle during cell division (Figure 5D,E) [87]. It is thus vitally important for the cell to control the centrosome's number and size, which can be accomplished by autocatalytic droplets with an active core. While the activation of building blocks inside the droplets leads to the experimentally observed sigmoidal growth behavior (Figure 5D; i.e., the exponential growth plateaus), the number of active cores in the cell regulates how many centrosomes are formed (Figure 5E) [84].

Design 3: activation outside and deactivation outside

In this design, activation and deactivation occur outside of the droplets. Boekhoven and colleagues demonstrated this design using the carbodiimide fuel-driven reaction cycle that transiently activates an anionic diacid into an uncharged anhydride. When the building block has a hydrophobic tail (i.e., a chain of six to ten carbons), it is soluble, yet it phase-separates into oil droplets upon activation (Figure 6A) [88]. Since the fuel, deactivated building block, and water are excluded from the oil phase, activation and deactivation occur in the dilute phase. An attractive unique property emerges from this design. Because the deactivation occurs outside of the droplets, the droplets are essentially 'protecting' their activated building blocks from the deactivation [89]. As a result, the deactivation only occurs on the fraction of activated building blocks that are present in the solution, which is equal to their solubility. Therefore, the deactivation rate equals the deactivation rate constant multiplied by the solubility. Because both factors are constant, the deactivation rate is also constant (i.e., zero-order deactivation). Moreover, the rate decreases with decreasing solubility of the activated building blocks. When the levels of these activated building blocks decay over time when a finite amount of fuel is added, their decay profiles differ. Indeed, when the activated building blocks cannot phase-separate, they decay with pseudo-first-order kinetics, which is the case for C_6-succinic anhydride (Figure 6B, green trace) [90]. In contrast, for the droplet-forming C_8-succinic anhydride (red), the deactivation kinetics follow a zero-order reaction (i.e., the activated building blocks deactivate with linear kinetics after all fuel is depleted). Moreover, the zero-order rate of deactivation scales with the solubility of the activated building block. In other words, the poorly soluble C_{10}-succinic anhydride deactivates drastically slower than C_8-succinic anhydride. Excitingly, this self-protection mechanism can be applied as transient emulsions that deliver hydrophobic drugs with linear decay kinetics [90]. Also, this feedback mechanism provides access to parasitic behavior in which molecules that partition into droplets benefit from the protective environment [91].

Another consequence of this design is that Ostwald ripening can be accelerated. Boekhoven and colleagues observed this behavior when they maintained these anhydride-based oil droplets in a steady state by continuously pipetting in chemical fuel. For example, when C_8-succinic acid droplets were actively maintained with a constant flux of 60 μM/min fuel, the droplets coarsened into a few large droplets within 2 h without any evidence of droplet fusion (Figure 6C) [33]. This ripening behavior is considerably faster than the Ostwald ripening of passive droplets with similar interfacial surface tension and solubility. Moreover, the ripening rate was correlated to the deactivation rate of the activated building blocks (i.e., a higher deactivation rate led to a faster ripening of droplets; Figure 6D) [33]. The authors found that the ripening of these active droplets was accelerated by up to two orders of magnitude compared with Ostwald ripening of passive droplets (Figure 6E) [33].

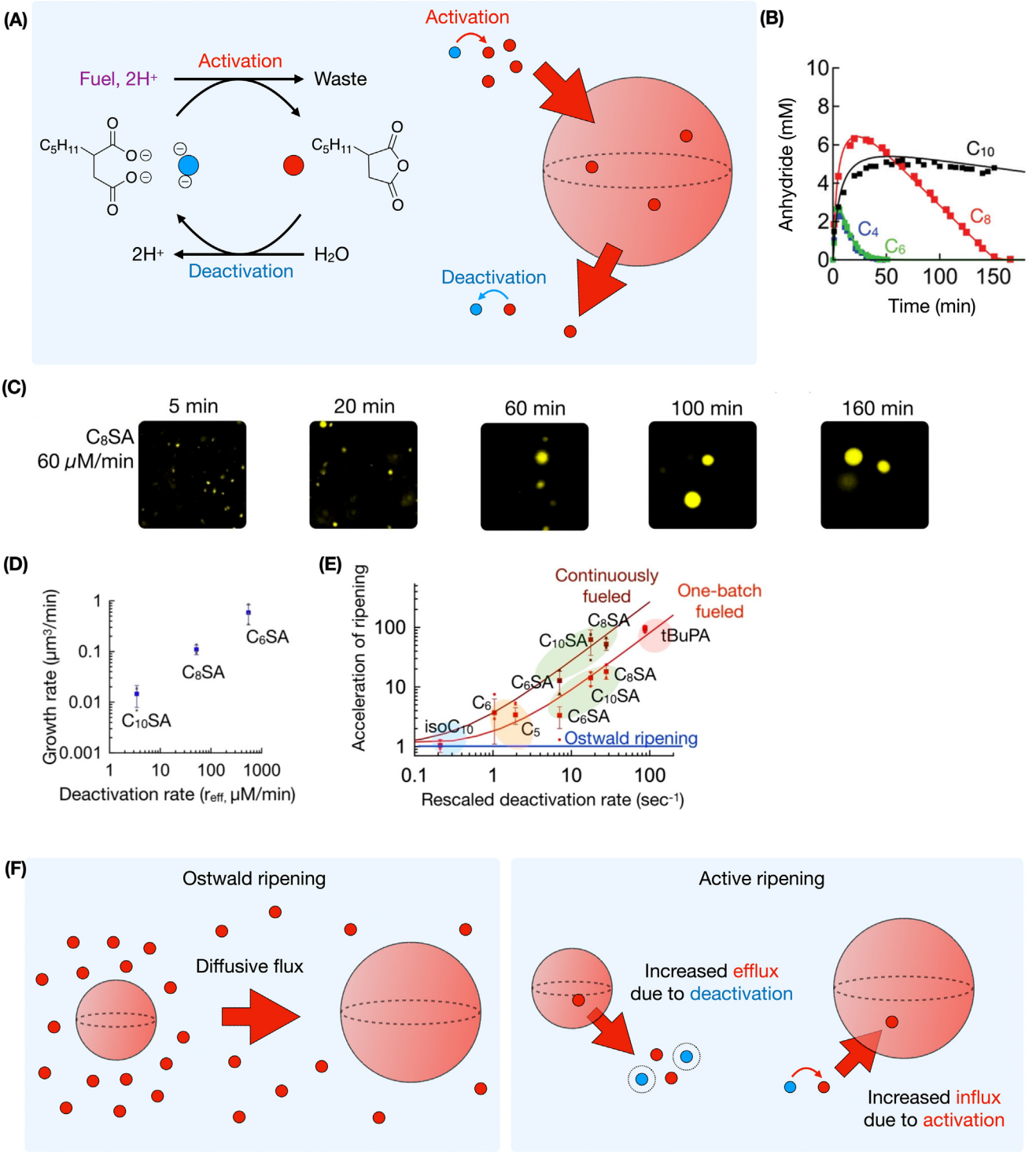

Figure 6. Carbodiimide-fueled droplets following design 3. (A) A chemical reaction cycle converts a chemical fuel (EDC) into waste (EDU) and transiently removes two negative charges on a molecule with a hydrophobic tail [89]. A schematic representation of a droplet where a building block is activated and deactivated in the dilute

(Figure legend continued at the bottom of the next page.)

Boekhoven and colleagues explained the acceleration of Ostwald ripening by an increased flux between small and large droplets (Figure 6F). They embedded the experimental results into a theoretical framework. As mentioned earlier, Ostwald ripening is driven by a concentration gradient between small and large droplets caused by Laplace pressure differences. Specifically, small droplets have a high concentration of building blocks around them. In contrast, large droplets are surrounded by a lower concentration of building blocks due to a lower Laplace pressure than smaller droplets. In chemically fueled droplets following design 3, the deactivation reaction occurs in the solution. It thus locally lowers the concentration gradient between small and large droplets. Lowering the gradient preferentially removes activated building blocks from small droplets with a high Laplace pressure. In other words, the probability that the deactivated molecule is substituted from a molecule from a small droplet is higher than that from a large droplet. In contrast, activation creates new activated building blocks on the concentration gradient. That excess activated building block is more likely to diffuse down the concentration gradient into larger droplets with a low Laplace pressure. Taken together, activation accelerates the growth of large droplets. Deactivation preferentially dissolves small droplets. As a result, both reactions contributed to an accelerated ripening until, eventually, only one droplet remained. Unlike droplet designs 1 and 2, this design cannot lead to a stable emulsion.

Design 4: activation inside and deactivation inside

Lastly, we discuss the design where droplet building blocks are activated and deactivated inside the droplets. While theory-based work is scarce on droplets following design 4, Deng and Walther reported an experimental approach based on coacervate droplets that comprise DNA (Figure 7A,B) [92]. Specifically, DNA-based constructs with complementary sticky ends were activated via ligation and deactivated through cleavage by an enzyme pair, T4 DNA ligase and BsaI, respectively, resulting in transient elongation of DNA strands. The distance between identical and complimentary sticky ends could tune the multivalency, leading to droplets with a broad strand length distribution of up to 1500 base pairs.

Droplets that survived for up to 2 days could be formed, depending on the amount of ATP added. The authors provided experiments that allow estimating where activation and deactivation took place. First, it was demonstrated that new monomers added to preformed fuel-driven droplets were incorporated into the droplet phase within hours (Figure 7C) [92]. This activation of freshly supplied building blocks shows the dynamic reshuffling in this droplet system, which indicates that activation occurs in the droplet. Secondly, individual droplets formed vacuoles, indicating that activated building blocks were deactivated within the droplet. Finally, the authors demonstrated that the interactions of complementary sticky ends of DNA are highly specific, allowing for self-sorting mechanisms where droplets made from differently constructed monomers do not fuse and mix material. Such exciting behavior is typically not accessible to other aqueous droplets, such as complex coacervates, composed of nonspecific electrostatic interactions.

Two other synthetic examples fulfill the criteria of activation and deactivation occurring inside the droplets. In these cases, the deactivation reaction was associated with morphological changes

phase. Since fuel and water are excluded from the droplet, activation and deactivation occur outside the droplet. (B) The concentration of activated building block (anhydride) with a varying hydrophobic tail as a function of time after adding 10 mM fuel. Markers represent HPLC data while lines represent fits from the kinetic model. Adapted, with permission, from [90]. (C) Confocal microscopy micrographs of C_8 succinic acid (building block) with continuous fueling of 60 μM/min fuel [33]. (D) Droplet growth rate as a function of the deactivation rate of succinic acid-based activated building blocks [33]. (E) Acceleration of ripening as a function of the deactivation rate for various activated building blocks. [33] The fueling mode and the deactivation rate regulate the degree of acceleration. (C–E) Adapted, with permission, from [33]. (F) Schematic representation of the mechanism of Ostwald ripening and active ripening. Due to Laplace pressure differences between small and large droplets, a concentration gradient between the droplets favors the growth of large droplets and the shrinkage of smaller ones. This process is accelerated if activation and deactivation are present in the dilute phase.

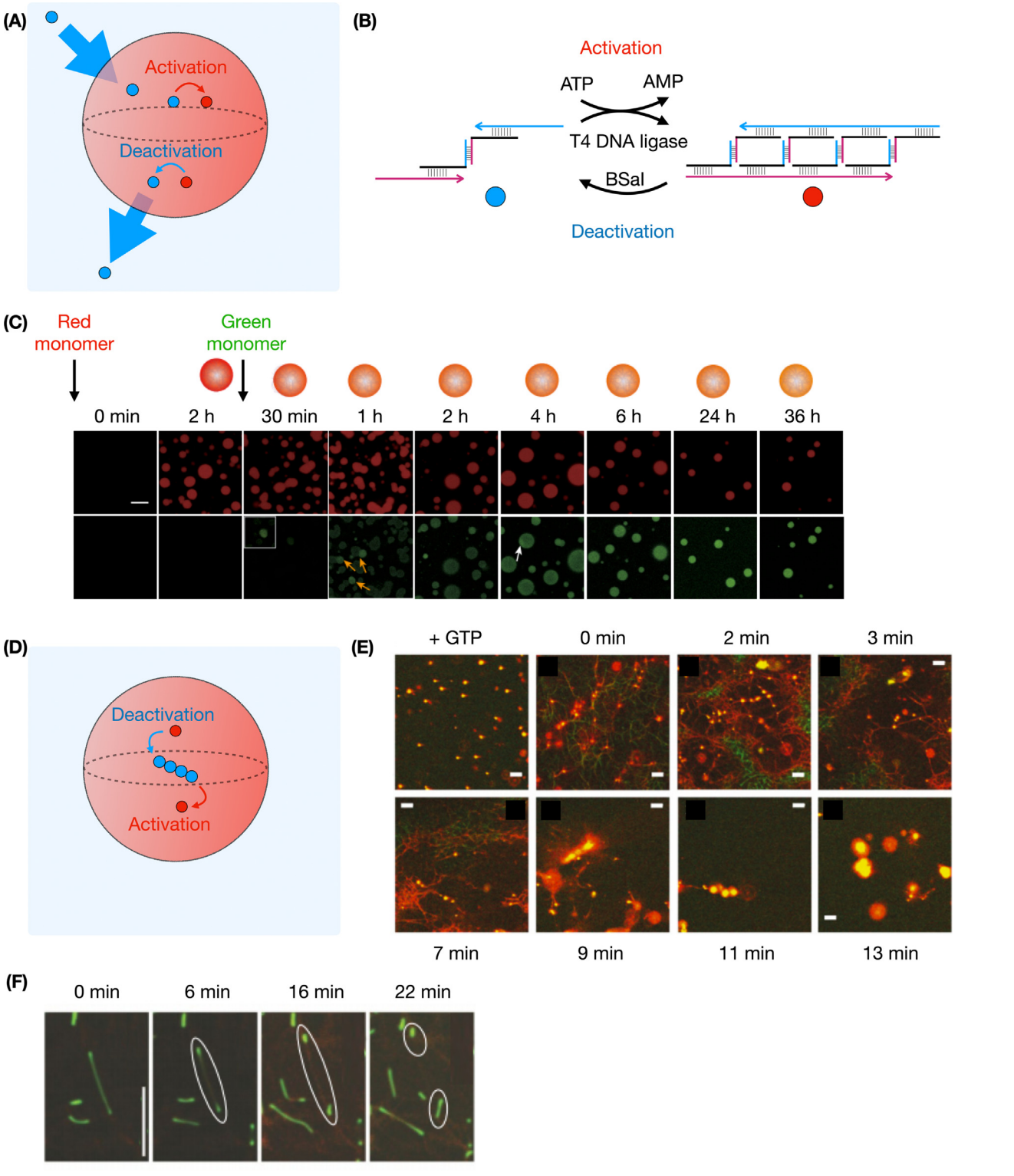

Trends in Chemistry

(See figure legend at the bottom of the next page.)

where activated building blocks were deactivated to form filaments within the droplets instead (Figure 7D). Monterroso and coworkers reported coacervate droplets composed of FtsZ and the SlmA protein, a biological inhibitor of FtsZ [93]. Adding GTP temporally transformed the droplets into fibrous structures (Figure 7E) [93]. These fibers are formed due to a stronger binding and stacking between FtsZ monomers when GTP is present [80,94]. In other words, in the presence of GTP, FtsZ as an activated building block was deactivated to assemble into fibers instead. Activation of FtsZ by GTP hydrolysis then restored the droplets within minutes.

Te Brinke and colleagues published the formation of FtsZ fibrils in GTP/polylysine complex coacervate droplets [95]. In this work, the amount of FtsZ and GTP influenced the change in the droplets' morphology (Figure 7F) [95]. At selected conditions, fibrils grew inside the droplets. These fibrils showed various growth, shrinkage, bending, and fusion behaviors. Excitingly, some fibrils split the original droplet in two. The authors explained this division process by a reaction-diffusion model where deformed droplets favor the elongation at the fibril ends. This is in line with simulations on self-dividing droplets [31,32].

Colocalizing both activation and deactivation of building blocks into liquid droplets may thus lead to exciting non-equilibrium behavior. Specifically, this experimental work shows the regulation of droplet morphology through chemical reactions, which should inspire us to build better liquid droplet models.

Concluding remarks

In recent years, the discovery of liquid droplets to organize molecules and biochemical reactions in the cytosol led to a better understanding of how today's cells regulate reaction cascades spatiotemporally. At the same time, a new interest in synthetic liquid droplets emerged as a model for these droplets in our cells and compartmentalization of prebiotic chemistry at the origin of life. Thus, for our fundamental understanding, it is crucial to build liquid droplet models regulated by chemical reactions.

We provided design considerations for chemically fueled droplets and outlined what unique properties can be expected. We considered four cases where chemical energy is dissipated to simultaneously activate and deactivate droplet building blocks. When activation and deactivation are colocalized in the same phase, we discussed accelerated ripening, droplets protecting their building blocks, and changes in the droplets' morphology. When activation and deactivation are delocalized, the droplet's size can be stable and even controlled. Large stationary sizes can result in self-dividing droplets. Increasing experimental work follows the design of this theory-based work and it will be exciting to see whether future experiments can confirm these predictions.

Despite the recent advances in the field, there are still many unknowns regarding the design of chemically fueled droplets (see Outstanding questions). On the one hand, experimentalists could better quantify where the reactions occur to connect theory and experiments. Also,

Outstanding questions

Can chemically fueled droplets be sustained in a steady state?

How can waste accumulation be prevented from affecting chemically fueled droplets?

Can phase-separated mixtures with more than two components be modeled theoretically?

How can numerical simulations account for the solvent in the phase separation process when chemical reactions are present?

Figure 7. ATP- and GTP-fueled droplets following design 4. (A) Schematic representation of a droplet where a building block is activated and deactivated inside the droplet. (B) A chemical reaction cycle where an enzyme pair activates (elongation) and deactivates (shortens) DNA strands inside the droplet at the expense of ATP [92]. In contrast to Figure 4, the activated building blocks are considerably larger than the building block monomers due to the polymerization reaction. (C) Dynamic incorporation of new DNA strands into DNA coacervates. Addition of new DNA strands (green, $ATTO_{488}$), 2 h after the formation of DNA coacervates (red, $ATTO_{647}$). Yellow arrows indicate inhomogeneous fluorescence within droplets due to fusion events that homogenize over several hours (white arrow). Scale bar: 20 μm. Adapted, with permission, from [92]. (D) Schematic representation of a droplet where an activated building block is deactivated to form filaments and reactivated inside the droplet. (E) Confocal micrographs of the transient reorganization of FtsZ coacervate droplets to fibers by adding GTP. Scale bar: 5 μm. Adapted, with permission, from [93]. (F) Confocal micrographs of a self-dividing fiber that grows from within droplets. Scale bar: 10 μm. Adapted, with permission, from [95].

numerical simulations usually operate at stationary states, unlike many experimental designs that work under conditions where the fuel is continuously depleting. Overcoming challenges such as waste accumulation will be one of the significant tasks in following theory-based work more closely. On the other hand, theoretical simulations need to account for parameters that cannot be neglected in experiments. For example, most numerical simulations focus on binary systems with only two molecular components. However, biomolecular condensates and coacervate droplets typically have more than one droplet component. Also, theory-based studies typically neglect the contribution of the fuel and the waste as a droplet component, which has been demonstrated as not always true in experimental work. Finally, most theory work does not consider the effect of the solvent on the phase separation process, which is now being gradually addressed [96]. Implementing these ideas into theory-based and experimental work will help us build better liquid droplet models for today and prebiotic cellular droplets.

Acknowledgments

The Boekhoven Lab is grateful for support from the Deutsche Forschungsgemeinschaft (DFG, German Research Foundation) through Project-ID 364653263 – TRR 235, Germany's Excellence Strategy - EXC-2094 – 390783311 (Origins), and for project 411722921. We are also grateful for the TUM Innovation Network - RISE funded through the Excellence Strategy. This research was conducted within the Max Planck School Matter to Life, supported by the German Federal Ministry of Education and Research (BMBF) in collaboration with the Max Planck Society. J.B. is grateful for funding from the European Research Council (ERC starting grant, ActiDrops) under 852187.

Declaration of interests

The authors have no competing financial interests to declare.

References

1. Flory, P.J. (1942) Thermodynamics of high polymer solutions. *J. Chem. Phys.* 10, 51–61
2. Huggins, M.L. (1942) Some properties of solutions of long-chain compounds. *J. Phys. Chem.* 46, 151–158
3. Bray, A.J. (1993) Theory of phase ordering kinetics. *Phys. A* 194, 41–52
4. Thiam, A.R. *et al.* (2013) The biophysics and cell biology of lipid droplets. *Nat. Rev. Mol. Cell Biol.* 14, 775–786
5. Hyman, A.A. *et al.* (2014) Liquid-liquid phase separation in biology. *Annu. Rev. Cell Dev. Biol.* 30, 39–58
6. Wang, H. *et al.* (2010) Altered lipid droplet dynamics in hepatocytes lacking triacylglycerol hydrolase expression. *Mol. Biol. Cell* 21, 1991–2000
7. Ariotti, N. *et al.* (2012) Postlipolytic insulin-dependent remodeling of micro lipid droplets in adipocytes. *Mol. Biol. Cell* 23, 1826–1837
8. Paar, M. *et al.* (2012) Remodeling of lipid droplets during lipolysis and growth in adipocytes. *J. Biol. Chem.* 287, 11164–11173
9. Yang, H. *et al.* (2012) Controlling the size of lipid droplets: lipid and protein factors. *Curr. Opin. Cell Biol.* 24, 509–516
10. Brangwynne, C.P. *et al.* (2011) Active liquid-like behavior of nucleoli determines their size and shape in *Xenopus laevis* oocytes. *Proc. Natl. Acad. Sci. U. S. A.* 108, 4334–4339
11. Griffin, E.E. *et al.* (2011) Regulation of the MEX-5 gradient by a spatially segregated kinase/phosphatase cycle. *Cell* 146, 955–968
12. Reineke, L.C. *et al.* (2017) Casein kinase 2 is linked to stress granule dynamics through phosphorylation of the stress granule nucleating protein G3BP1. *Mol. Cell. Biol.* 37, e00596-16
13. Hondele, M. *et al.* (2020) Membraneless organelles: phasing out of equilibrium. *Emerg. Top. Life Sci.* 4, 331–342
14. Gomes, E. and Shorter, J. (2019) The molecular language of membraneless organelles. *J. Biol. Chem.* 294, 7115–7127
15. Alberti, S. *et al.* (2019) Considerations and challenges in studying liquid-liquid phase separation and biomolecular condensates. *Cell* 176, 419–434
16. Elbaum-Garfinkle, S. (2019) Matter over mind: liquid phase separation and neurodegeneration. *J. Biol. Chem.* 294, 7160–7168
17. Spannl, S. *et al.* (2019) Biomolecular condensates in neurodegeneration and cancer. *Traffic* 20, 890–911
18. Alberti, S. and Hyman, A.A. (2021) Biomolecular condensates at the nexus of cellular stress, protein aggregation disease and ageing. *Nat. Rev. Mol. Cell Biol.* 22, 196–213
19. Defronzo, R.A. (2004) Dysfunctional fat cells, lipotoxicity and type 2 diabetes. *Int. J. Clin. Pract.* 143, 9–21
20. Bostrom, P. *et al.* (2007) SNARE proteins mediate fusion between cytosolic lipid droplets and are implicated in insulin sensitivity. *Nat. Cell Biol.* 9, 1286–1293
21. Sun, Z. *et al.* (2013) Perilipin1 promotes unilocular lipid droplet formation through the activation of Fsp27 in adipocytes. *Nat. Commun.* 4, 1594
22. Brangwynne, C.P. *et al.* (2009) Germline P granules are liquid droplets that localize by controlled dissolution/condensation. *Science* 324, 1729–1732
23. Seydoux, G. (2018) The P granules of *C. elegans*: a genetic model for the study of RNA-protein condensates. *J. Mol. Biol.* 430, 4702–4710
24. Shin, Y. and Brangwynne, C.P. (2017) Liquid phase condensation in cell physiology and disease. *Science* 357, eaaf4382
25. Banani, S.F. *et al.* (2017) Biomolecular condensates: organizers of cellular biochemistry. *Nat. Rev. Mol. Cell Biol.* 18, 285–298
26. Brangwynne, C.P. *et al.* (2015) Polymer physics of intracellular phase transitions. *Nat. Phys.* 11, 899–904
27. Rieß, B. *et al.* (2020) The design of dissipative molecular assemblies driven by chemical reaction cycles. *Chem* 6, 552–578
28. Zwicker, D. *et al.* (2015) Suppression of Ostwald ripening in active emulsions. *Phys. Rev. E Stat. Nonlinear Soft Matter Phys.* 92, 012317
29. Wurtz, J.D. and Lee, C.F. (2018) Chemical-reaction-controlled phase separated drops: formation, size selection, and coarsening. *Phys. Rev. Lett.* 120, 078102
30. Weber, C.A. *et al.* (2019) Physics of active emulsions. *Rep. Prog. Phys.* 82, 064601
31. Zwicker, D. *et al.* (2016) Growth and division of active droplets provides a model for protocells. *Nat. Phys.* 13, 408–413
32. Seyboldt, R. and Jülicher, F. (2018) Role of hydrodynamic flows in chemically driven droplet division. *New J. Phys.* 20, 105010

33. Tena-Solsona, M. *et al.* (2020) Accelerated ripening in chemically fueled emulsions. *ChemSystemsChem* 3, e20000034
34. Illien, P. *et al.* (2017) 'Fuelled' motion: phoretic motility and collective behaviour of active colloids. *Chem. Soc. Rev.* 46, 5508–5518
35. Meredith, C.H. *et al.* (2022) Chemical design of self-propelled Janus droplets. *Matter* 5, 616–633
36. Drobot, B. *et al.* (2018) Compartmentalised RNA catalysis in membrane-free coacervate protocells. *Nat. Commun.* 9, 3643
37. Poudyal, R.R. *et al.* (2019) Template-directed RNA polymerization and enhanced ribozyme catalysis inside membraneless compartments formed by coacervates. *Nat. Commun.* 10, 490
38. Martin, N. *et al.* (2017) Light-induced dynamic shaping and self-division of multipodal polyelectrolyte-surfactant microarchitectures via azobenzene photomechanics. *Sci. Rep.* 7, 41327
39. Martin, N. *et al.* (2019) Photoswitchable phase separation and oligonucleotide trafficking in DNA coacervate microdroplets. *Angew. Chem. Int. Ed.* 58, 14594–14598
40. Wee, W.A. *et al.* (2021) Photoswitchable single-stranded DNA-peptide coacervate formation as a dynamic system for reaction control. *iScience* 24, 103455
41. Merindol, R. *et al.* (2021) Fast and ample light controlled actuation of monodisperse all-DNA microgels. *Adv. Funct. Mater.* 31, 2010396
42. Reed, E.H. and Hammer, D.A. (2018) Redox sensitive protein droplets from recombinant oleosin. *Soft Matter* 14, 6506–6513
43. Matsuo, M. and Kurihara, K. (2021) Proliferating coacervate droplets as the missing link between chemistry and biology in the origins of life. *Nat. Commun.* 12, 5487
44. Abbas, M. *et al.* (2021) A short peptide synthon for liquid-liquid phase separation. *Nat. Chem.* 13, 1046–1054
45. Koga, S. *et al.* (2011) Peptide-nucleotide microdroplets as a step towards a membrane-free protocell model. *Nat. Chem.* 3, 720–724
46. Cingil, H.E. *et al.* (2018) Temporally programmed disassembly and reassembly of C3Ms. *Small* 14, 1802089
47. Love, C. *et al.* (2020) Reversible pH-responsive coacervate formation in lipid vesicles activates dormant enzymatic reactions. *Angew. Chem. Int. Ed.* 59, 5950–5957
48. Garenne, D. *et al.* (2016) Sequestration of proteins by fatty acid coacervates for their encapsulation within vesicles. *Angew. Chem. Int. Ed.* 55, 13475–13479
49. Krishna Kumar, R. *et al.* (2016) Self-transformation and structural reconfiguration in coacervate-based protocells. *Chem. Sci.* 7, 5879–5887
50. Douliez, J.P. *et al.* (2017) Catanionic coacervate droplets as a surfactant-based membrane-free protocell model. *Angew. Chem. Int. Ed.* 56, 13689–13693
51. Martin, N. *et al.* (2018) Antagonistic chemical coupling in self-reconfigurable host-guest protocells. *Nat. Commun.* 9, 3652
52. Nichols, M.K. *et al.* (2018) Fabrication of micropatterned dipeptide hydrogels by acoustic trapping of stimulus-responsive coacervate droplets. *Small* 14, e1800739
53. Qiao, Y. *et al.* (2019) Response-retaliation behavior in synthetic protocell communities. *Angew. Chem. Int. Ed.* 58, 17758–17763
54. Spruncken, C.C.M. *et al.* (2020) Two-stage polyelectrolyte assembly orchestrated by a clock reaction. *ChemSystemsChem* 2, e2000005
55. Karoui, H. *et al.* (2021) Self-programmed enzyme phase separation and multiphase coacervate droplet organization. *Chem. Sci.* 12, 2794–2802
56. Banerjee, P.R. *et al.* (2017) Reentrant phase transition drives dynamic substructure formation in ribonucleoprotein droplets. *Angew. Chem. Int. Ed.* 56, 11354–11359
57. Schuster, B.S. *et al.* (2018) Controllable protein phase separation and modular recruitment to form responsive membraneless organelles. *Nat. Commun.* 9, 2985
58. Aumiller, W.M., Jr and Keating, C.D. (2016) Phosphorylation-mediated RNA/peptide complex coacervation as a model for intracellular liquid organelles. *Nat. Chem.* 8, 129–137
59. Nakashima, K.K. *et al.* (2018) Reversible generation of coacervate droplets in an enzymatic network. *Soft Matter* 14, 361–367
60. Yang, S. *et al.* (2019) Steering coacervation by a pair of broad-spectrum regulators. *ACS Nano* 13, 2420–2426
61. Deshpande, S. *et al.* (2019) Spatiotemporal control of coacervate formation within liposomes. *Nat. Commun.* 10, 1800
62. Spoelstra, W.K. *et al.* (2020) Nonspherical coacervate shapes in an enzyme-driven active system. *Langmuir* 36, 1956–1964
63. Zhou, L. *et al.* (2021) A multiresponsive transformation between surfactant-based coacervates and vesicles. *CCS Chem.* 3, 358–366
64. Nakashima, K.K. *et al.* (2021) Active coacervate droplets are protocells that grow and resist Ostwald ripening. *Nat. Commun.* 12, 3819
65. Wang, L. *et al.* (2019) Autonomic behaviors in lipase-active oil droplets. *Angew. Chem. Int. Ed.* 58, 1067–1071
66. Shimokuri, T. *et al.* (2006) Effects of thermoresponsive coacervation on the hydrolytic degradation of amphipathic poly(gamma-glutamate)s. *Macromol. Biosci.* 6, 942–951
67. Ding, Y. *et al.* (2019) Polymerization-induced self-assembly promoted by liquid–liquid phase separation. *ACS Macro Lett.* 8, 943–946
68. Jia, T.Z. *et al.* (2019) Membraneless polyester microdroplets as primordial compartments at the origins of life. *Proc. Natl. Acad. Sci. U. S. A.* 116, 15830–15835
69. Wang, J. *et al.* (2021) Selective amide bond formation in redox-active coacervate protocells. *ChemRxiv* Published online August 27, 2021. https://doi.org/10.26434/chemrxiv-2021-1zt9k
70. Fraccia, T.P. and Martin, N. (2021) Non-enzymatic oligonucleotide ligation in photoswitchable coacervate protocells sustains compartment-content coupling. *ChemRxiv* Published online December 9, 2021. https://doi.org/10.26434/chemrxiv-2021-zg20r
71. Martin, M. *et al.* (2007) Fatty acid chemistry at the oil–water interface: self-propelled oil droplets. *J. Am. Chem. Soc.* 129, 9386–9391
72. Chen, H. *et al.* (2020) One-step dynamic imine chemistry for preparation of chitosan-stabilized emulsions using a natural aldehyde: acid trigger mechanism and regulation and gastric delivery. *J. Agric. Food Chem.* 68, 5412–5425
73. Blocher, W.C. and Perry, S.L. (2017) Complex coacervate-based materials for biomedicine. *Wiley Interdiscip. Rev. Nanomed. Nanobiotechnol.* 9, 27813275
74. Martin, N. (2019) Dynamic synthetic cells based on liquid-liquid phase separation. *Chembiochem* 20, 2553–2568
75. Cejkova, J. *et al.* (2017) Droplets as liquid robots. *Artif. Life* 23, 528–549
76. Suematsu, N.J. and Nakata, S. (2018) Evolution of self-propelled objects: from the viewpoint of nonlinear science. *Eur. J. Chem.* 24, 6308–6324
77. Zwicker, D. (2022) The intertwined physics of active chemical reactions and phase separation. *arXiv* Published online Feb 28, 2022. https://doi.org/10.48550/arXiv.2202.13646
78. Golestanian, R. (2017) Division for multiplication. *Nat. Phys.* 13, 323–324
79. Fanalista, F. *et al.* (2018) FtsZ-induced shape transformation of coacervates. *Adv. Biosyst.* 2, 1800136
80. Mukherjee, A. and Lutkenhaus, J. (1998) Dynamic assembly of FtsZ regulated by GTP hydrolysis. *EMBO J.* 17, 462–469
81. Donau, C. *et al.* (2020) Active coacervate droplets as a model for membraneless organelles and protocells. *Nat. Commun.* 11, 5167
82. Spath, F. *et al.* (2021) Molecular design of chemically fueled peptide-polyelectrolyte coacervate-based assemblies. *J. Am. Chem. Soc.* 143, 4782–4789
83. Bergmann, A.M. *et al.* (2022) Evolution and single-droplet analysis of fuel-driven compartments by droplet-based microfluidics. *Angew. Chem. Int. Ed.*, e202203928
84. Zwicker, D. *et al.* (2014) Centrosomes are autocatalytic droplets of pericentriolar material organized by centrioles. *Proc. Natl. Acad. Sci. U. S. A.* 111, E2636–E2645
85. Zwicker, D. *et al.* (2018) Positioning of particles in active droplets. *Phys. Rev. Lett.* 121, 158102
86. Decker, M. *et al.* (2011) Limiting amounts of centrosome material set centrosome size in *C. elegans* embryos. *Curr. Biol.* 21, 1259–1267
87. Woodruff, J.B. (2021) The material state of centrosomes: lattice, liquid, or gel? *Curr. Opin. Struct. Biol.* 66, 139–147
88. Tena-Solsona, M. *et al.* (2017) Non-equilibrium dissipative supramolecular materials with a tunable lifetime. *Nat. Commun.* 8, 15895
89. Tena-Solsona, M. *et al.* (2018) Self-selection of dissipative assemblies driven by primitive chemical reaction networks. *Nat. Commun.* 9, 2044

90. Wanzke, C. *et al.* (2020) Active droplets in a hydrogel release drugs with a constant and tunable rate. *Mater. Horiz.* 7, 1397–1403
91. Schwarz, P.S. *et al.* (2021) Parasitic behavior in competing chemically fueled reaction cycles. *Chem. Sci.* 12, 7554–7560
92. Deng, J. and Walther, A. (2020) Programmable ATP-fueled DNA coacervates by transient liquid-liquid phase separation. *Chem* 6, 3329–3343
93. Monterroso, B. *et al.* (2019) Bacterial FtsZ protein forms phase-separated condensates with its nucleoid-associated inhibitor SlmA. *EMBO Rep.* 20, e45946
94. Chen, Y. and Erickson, H.P. (2005) Rapid in vitro assembly dynamics and subunit turnover of FtsZ demonstrated by fluorescence resonance energy transfer. *J. Biol. Chem.* 280, 22549–22554
95. Te Brinke, E. *et al.* (2018) Dissipative adaptation in driven self-assembly leading to self-dividing fibrils. *Nat. Nanotechnol.* 13, 849–855
96. Bauermann, J. *et al.* (2022) Energy and matter supply for active droplets. *Rxiv* Published online March 14, 2022. https://doi.org/10.48550/arXiv.2203.07528